



## Charge density of difluorides from synchrotron diffraction data and investigation of bonding in low valent binary fluorides

K. Sujatha<sup>a,b</sup>, S. Israel<sup>b,\*</sup>, C. Anzline<sup>a,b</sup>, R.A.J.R. Sheeba<sup>b</sup>

<sup>a</sup> Mother Teresa Women's University, Kodaikanal, 624 102, Tamil Nadu, India

<sup>b</sup> Department of Physics, The American College, Madurai, 625 002, India

### HIGHLIGHTS

- Accurate Synchrotron single crystal X – ray data is used for the study of charge density distribution in CoF<sub>2</sub> and NiF<sub>2</sub>.
- Fluorine bonding with metals of different oxidation state of metal cations ranging from +1 to +3 is thoroughly analysed.
- The population and kappa parameters were refined and studied using multipole model of charge density estimation.
- The (3,-1) Bond Critical Points are determined and thus the topology of the charge density is analysed.
- Maximum Entropy Method is adopted for a clear visualization of charge densities in the bonding regions.

### ARTICLE INFO

#### Keywords:

Charge density  
Synchrotron X-ray diffraction  
Multipole model  
MEM model  
Intermediate interaction

### ABSTRACT

The experimental charge density analysis of two isostructural transition metal difluorides, CoF<sub>2</sub> and NiF<sub>2</sub> has been performed using single crystal synchrotron X-ray diffraction data. The multipole and MEM models of electron density and the thermal vibration parameters suggest that the difluoride of nickel is a hard molecule with more shared shell interaction nature than the difluoride of cobalt. In the course of study, a comparative study on fluorine bonding in low valent binary fluorides with metal cations of oxidation states, ranging from +1 to +3 have been accomplished and thoroughly analysed. The explored topological features derived from the Bader's theory of Atoms In Molecules (AIM) approach reveals the existence of ionic nature of bonding at +1 valence state of metal, as viewed in LiF and NaF and as the oxidation on metals ascends, intermediate interaction with increase in covalent nature is evidenced.

### 1. Introduction

The entire society of scientists and technologists has recognized fluorides and oxides as two common choices concerning the selection of materials in research as well as in industries [1] due to their peculiar and intriguing physical, chemical, mechanical, optical, electrical and electronic properties. Indeed, the two attributes of these materials, i.e., their charming properties and its resultant amazing applications [2–15] are direct results of the high electronegative character of fluorine and oxygen [16,17]. In particular, compared to oxygen, fluorine is the most electronegative element and the least polarisable anion with relatively small atomic size. Moreover, it has the capability of forming stable fluorides, with strong bonds, with almost all the metals in the periodic table. Obviously, binary fluorides are compounds that contain at least

one fluorine atom and one other element in its chemical formula. Metal fluorides are harder when compared to its other corresponding halide compounds [18,19]. In actual fact almost all the properties of fluorides are determined mainly by its bonding motifs. The most important concept of oxidation states is the general and fundamental ordering of bonding principles in fluorides. In general, in all binary fluorides, fluorine exist in an oxidation state of –1 and the oxidation state of cation ranges from +1 to +6 [20–25]. According to Andrew R. Barron [20], these materials are mostly ionic in low valence states of cations, where as, they lean to be polar covalent in high valence states.

A series of recent experiments by our laboratory and collaborators, on the charge density analysis of monofluorides of lithium and sodium [26] and trifluorides of gallium and vanadium [27] have thrown new light on the bonding motifs of binary fluorides. It is thus shown that the

\* Corresponding author.

E-mail address: [israel.samuel@gmail.com](mailto:israel.samuel@gmail.com) (S. Israel).

<https://doi.org/10.1016/j.matchemphys.2020.123990>

Received 13 April 2020; Received in revised form 17 September 2020; Accepted 26 October 2020

Available online 2 November 2020

0254-0584/© 2020 Elsevier B.V. All rights reserved.

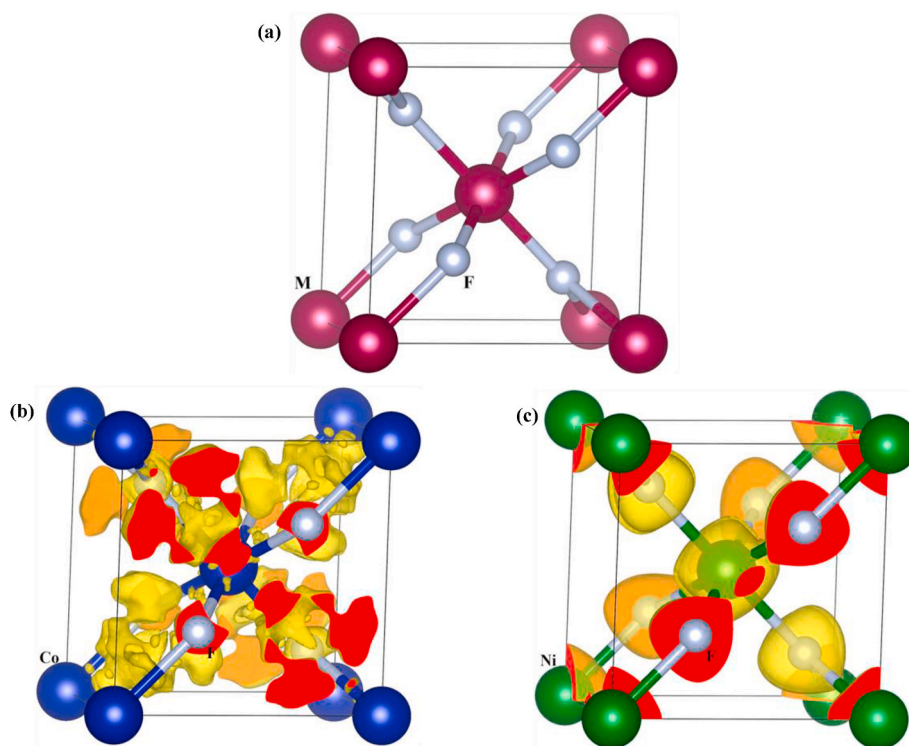


Fig. 1. (a). Isostructural unit cell of MF<sub>2</sub> (M = Co and Ni). 3- dimensional charge density distribution in (a) CoF<sub>2</sub> and (c) NiF<sub>2</sub> unit cell. The isosurface level is 1.0 e/Å<sup>3</sup>.

Table 1  
Summary of structure refinement.

Parameters	CoF <sub>2</sub>		NiF <sub>2</sub>	
	Present work	[50]	Present work	[50]
a (Å)	4.6956 (3)	4.6950 (7)	4.6298 (5)	4.6497 (6)
b (Å)	4.6956 (3)	4.6950 (7)	4.6298 (5)	4.6497 (6)
c (Å)	3.1793 (1)	3.1817 (5)	3.0693 (8)	3.0836 (6)
Cell Volume(Å <sup>3</sup> )	70.11 (6)	70.10	65.79 (6)	66.67
Density (gm/cc)	4.5920	4.590	4.8790	4.818
B <sub>iso</sub> (Å <sup>2</sup> )	0.54504 (2)	–	0.43469 (5)	–
B <sub>F</sub> (Å <sup>2</sup> )	0.82821 (5)	–	0.73568 (8)	–
R <sub>obs</sub> (%)	1.81	1.9	1.25	1.3
wR <sub>obs</sub> (%)	2.14	2.6	1.76	1.7
GOF	1.08	–	1.89	–

electron density analysis, when discussed with the aid of the two best possible and reliable methods, multipole and MEM (Maximum Entropy method) has the ability to afford an analytical description of electronic structures, chemical bonding and the correlations between them [28–30] and provide evidence in regard to a number of questions related to the properties of the fluorides [26,27]. In this regime, this thorough investigation on these monofluorides and trifluorides by electron density calculations has created a quest to perform the same methodology of analysis on difluorides also.

Transition metal difluorides is a persistent hot topic of research owing to their interesting optical and magnetic properties and applicability as potential materials in energy storage and catalysis [22,31–34]. Ardent knowledge about the crystal structures is a basic requirement for understanding the properties, especially the bonding characteristics of difluorides. TM difluorides, in general, adopt four types of structures, which comprise (i) tetragonal rutile type structure, such as FeF<sub>2</sub> and

Table 2  
Isotropic and anisotropic parameters.

Molecules	Atoms	Reference	B <sub>iso</sub> (Å <sup>2</sup> )	U <sub>11</sub>	U <sub>22</sub>	U <sub>33</sub>	U <sub>12</sub>	U <sub>13</sub>	U <sub>23</sub>
CoF <sub>2</sub>	Co	Present work	0.54504 (2)	0.00671 (4)	0.00671 (4)	0.00732 (5)	–0.00063 (3)	0.00000	0.00000
		[34]	0.50008 (4)	0.00685 (6)	0.00685 (6)	0.00533 (7)	–0.00073 (5)	0.00000	0.00000
		[50]	–	0.00696 (3)	–	0.00518 (2)	–0.00075 (62)	–	–
		[51]	–	0.00695 (4)	–	0.00532 (4)	–0.00076 (9)	–	–
	F	Present work	0.82821 (5)	0.01048 (8)	0.01048 (8)	0.01055 (2)	–0.00478 (3)	0.00000	0.00000
		[34]	0.83846 (17)	0.01193 (16)	0.01193 (16)	0.00803 (22)	–0.00529 (21)	0.00000	0.00000
		[50]	–	0.01263 (20)	–	0.00839 (29)	–0.01054(56)	–	–
		[51]	–	0.01162 (10)	–	0.00790 (11)	–0.00480 (15)	–	–
NiF <sub>2</sub>	Ni	Present work	0.43469 (5)	0.00596 (8)	0.00596 (8)	0.00461 (3)	–0.00024 (7)	0.00000	0.00000
		[47]	–	0.00500 (3)	–	0.00384 (5)	–0.00036 (3)	–	–
		[48]	–	0.00581 (2)	–	0.00485 (4)	–0.00017 (12)	–	–
		[50]	–	0.00526 (2)	–	0.00423 (4)	–0.00020 (42)	–	–
	F	Present work	0.73568 (8)	0.01052 (2)	0.01052 (2)	0.00695 (6)	–0.00906 (1)	0.00000	0.00000
		[47]	–	0.00939 (5)	–	0.00615 (6)	–0.00428 (5)	–	–
		[48]	–	0.01031 (12)	–	0.00729 (19)	–0.00446 (15)	–	–
		[50]	–	0.01025 (16)	–	0.00691 (24)	–0.00921 (46)	–	–

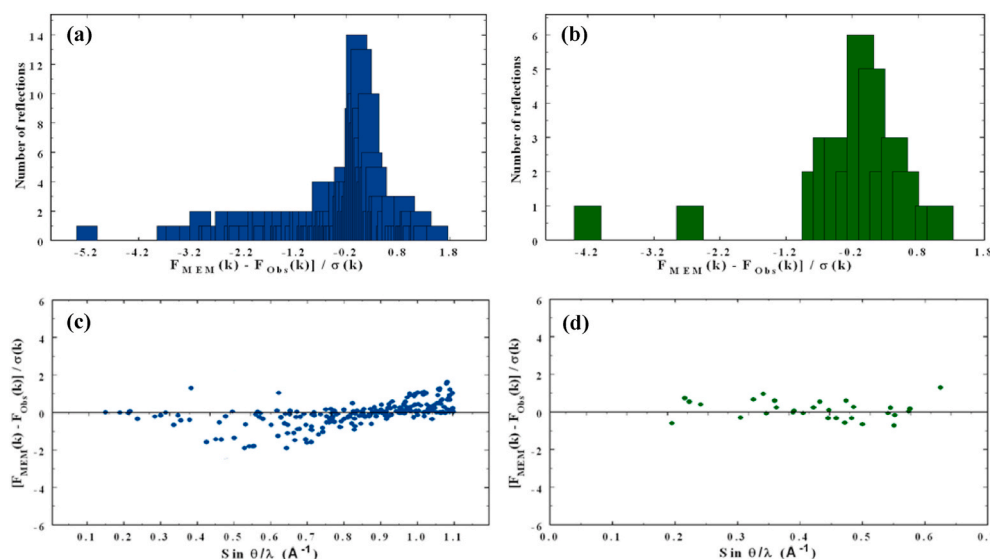


Fig. 2. Histogram of observed number of reflections of (a) CoF<sub>2</sub> and (b) NiF<sub>2</sub>. Error distribution of observations in the reciprocal space of (c) CoF<sub>2</sub> and (d) NiF<sub>2</sub>.

**Table 3**  
Summary of Charge density refinements.

Summary of MEM refinements				
Parameters	CoF <sub>2</sub>	NiF <sub>2</sub>		
Lagrange parameter	0.145500	0.002224		
Number of cycles	174	192		
Total charges in the unit cell	90.00	92.00		
Prior electron density (e/Å <sup>3</sup> )	1.2839	1.3982		
Resolution (eÅ <sup>-3</sup> /pixel)	0.05	0.05		
R <sub>obs</sub> (%)	1.26	1.07		
wR <sub>obs</sub> (%)	2.63	1.15		
Core and valence populations derived from kappa refinements				
	Co	F	Ni	F
P <sub>C</sub>	18.0282	1.9962	18.0112	2.0025
P <sub>V</sub>	8.1048	7.4476	9.6841	7.3829
K	1.0251	0.9903	1.0536	0.9542
κ'	1.0000	1.0000	1.0000	1.0000

MnF<sub>2</sub> (ii) cubic fluorite structure, typified by CdF<sub>2</sub> and HgF<sub>2</sub>; (iii) monoclinic structure, e.g. CrF<sub>2</sub> and CuF<sub>2</sub> and (iv) orthorhombic structure typified by AgF<sub>2</sub> [32–48]. For our present study, fluorides of two transition metals, cobalt and nickel (CoF<sub>2</sub>, NiF<sub>2</sub>) are elected as two representative members of a large family of difluorides. These low valent transition metal difluorides fall into the first category of crystal structure discussed above, i.e., tetragonal rutile type structure with *P4<sub>2</sub>/mnm* space group symmetry [37–56]. The isostructural unit cell of MF<sub>2</sub> (M = Co, Ni) is shown in Fig. 1(a). Here each metal atom is coordinated to six fluorine atoms and each fluorine atom is connected to three metal atoms.

Several articles and reports on the subject of Cobalt (II) fluoride and Nickel (II) fluoride, (related to their crystal structures, magnetic, vibrational and optical properties) have been published [31–33,37–47, 49,52–59]. In spite of the few charge density works reported [34,48,50, 51], the main focus of the authors was to relate the observed density maps to transition metal 3d orbital occupations and orbital splitting. Moreover two opposite outlooks exist between the fluoride researchers in rationalizing the bonding characteristics of these fluorides. One is that, Costa et al. [50] predict covalency effects in bonding, in CoF<sub>2</sub> and NiF<sub>2</sub>. The other is, in contrast, Nicholas J.O' Toole et al. [34], Palmer et al. [48], Jauch et al. [51]. and Brown et al. [56]. have emphasized a pure ionic type of bonding. These reports point out the stipulation to file the degree of ionicity and the amount of covalence mixing in cobalt difluoride and nickel difluoride. The advance in understanding of these phenomena requires the combined efforts of two most successful and

accurate methods, viz., multipole and MEM analysis of electron density estimation, which seems to be lacking in all the above reports. In fact, Palmer et al. [48]. has mentioned his failure in analysing the Maximum Entropy Method of charge density study in NiF<sub>2</sub> system. Therefore well organized investigations on these systems are indispensable to accomplish solid foundations in this regard. An extensive synchrotron x-ray analysis of charge density research efforts in two different paths (multipole and MEM) is focused to elucidate the bonding mechanisms in these binary fluorides. Further, our previous study on oxygen bonding with metals of different oxidation states has revealed several interesting as well as important facts on the bonding principles of binary oxides [60]. This prompted us to undertake a similar study on fluorine bonding with metals on low valence states of +1, +2 and +3. The present synchrotron study, therefore, has a twofold objective: (i) a precise study on bonding principles in both the crystals of CoF<sub>2</sub> and NiF<sub>2</sub> and (ii) an accurate elucidation of the trend of bonding character in low valent binary fluorides by correlating our present results on difluorides with the outcomes of Israel et al. on monofluorides [26] and our own previous consequences on trifluorides [27].

## 2. Crystallization and synchrotron X – ray data collection

Both CoF<sub>2</sub> and NiF<sub>2</sub> crystals are grown from the melt. The former is grown by the same method as accounted by Nicholas J.O' Toole et al. [34]. Reagent-grade CoF<sub>2</sub> powder is heated at a temperature of 800 °C in sealed platinum crucibles. By cooling the melt rapidly, small crystals of cobalt difluoride are formed. The latter is grown by the modified stockbarger method, tested and reported by Guggenheim [61] and Barbara M.Wanklyn [62]. Crystals of NiF<sub>2</sub> is formed after preheating NiCl by passing HF at 850 °C in sealed Pt–Rh alloy tube.

Small spheres of CoF<sub>2</sub> and NiF<sub>2</sub> were prepared from bulk crystals using Nonius crystal spherizer, from which good quality crystals were chosen for synchrotron X – ray data collection. Selection of these small and good quality crystals results in the reduction of absorption and extinction effects. Synchrotron radiation has the combined advantages of overwhelming intensity with low divergence. Hence high resolution synchrotron single crystal X - ray diffraction data collected by using Beamline 14A (BL14A) diffractometer is utilized for the present study. This four-circle diffractometer at the Photon factory in Tsukuba, Japan, is equipped with a vertical wiggler, which produces vertically polarized synchrotron radiation. The radiation is made to propagate through a double Si(111) crystal monochromator and is focused by using a curved mirror. The polarization ratio, i.e., the ratio of the total incident beam

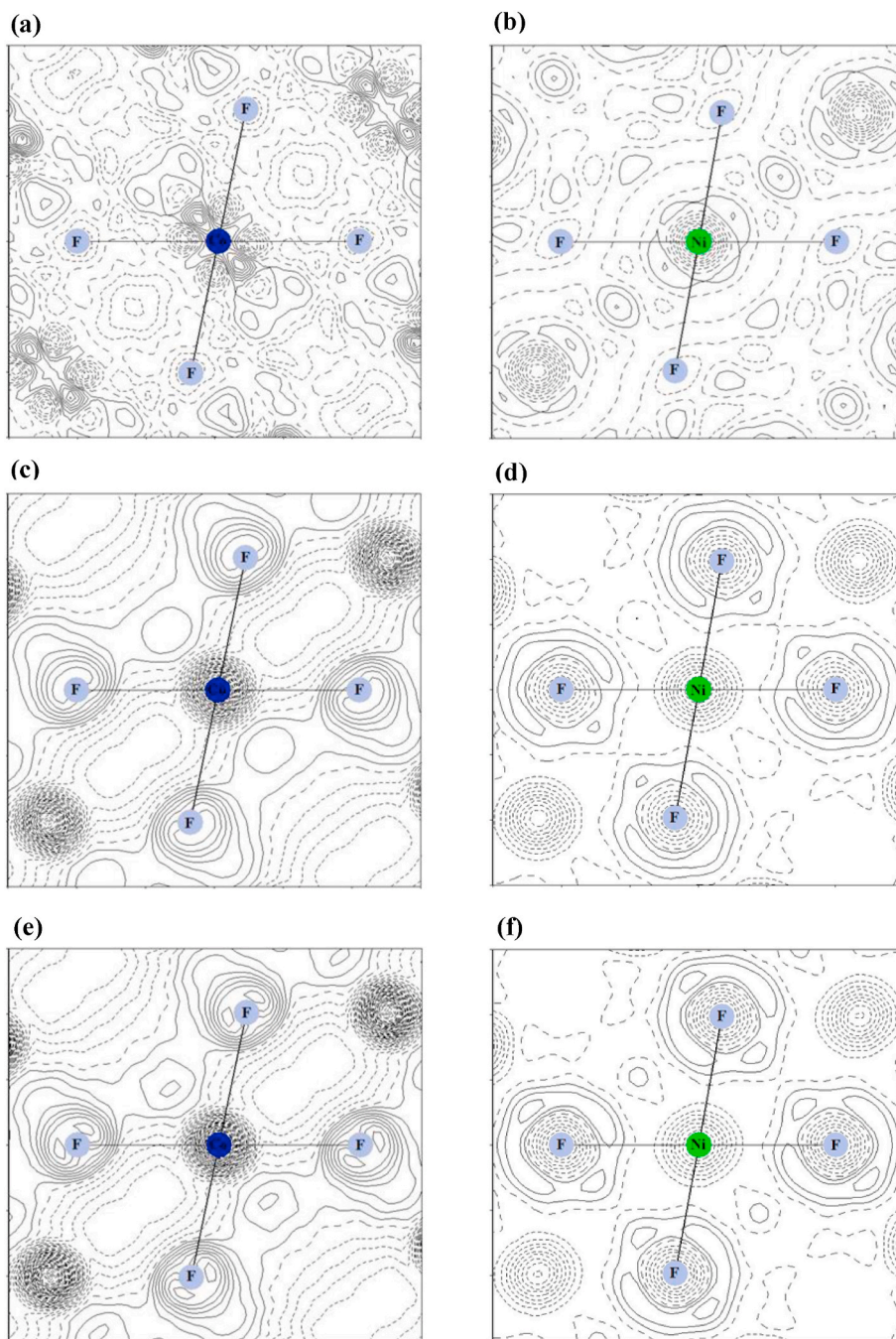


**Fig. 3.** Difference Fourier maps of (a) CoF<sub>2</sub> and (b) NiF<sub>2</sub>, Dynamic deformation multipole density maps of (c) CoF<sub>2</sub> and (d) NiF<sub>2</sub> and Static deformation multipole density maps of (e) CoF<sub>2</sub> and (f) NiF<sub>2</sub>. Negative contours are shown with dashed lines.

intensity to its electric vector vertical, is 0.95. A 0.4 mm incident beam slit, which is installed before the monitor ion-counter offers an intense and adequately homogeneous beam. The incident beam intensity is monitored by using an ion chamber, since the stored beam decays exponentially with time. During data collection, the arrangement of the first monochromator crystal and of the vertical translations of the mirror was optimized, every 20 min, by automatic flux maximizations. The effects due to the changes in the synchrotron radiation intensity, influenced by beam instabilities and thermal instability of the beamline optics are reduced by positioning the crystal slightly off the beam focus. Thus, an entire set of reflection data, with  $(\sin \theta/\lambda)_{\max} = 0.525 \text{ \AA}^{-1}$ ,  $-10 \leq h \leq 10$ ,  $-10 \leq k \leq 10$  and  $-6 \leq l \leq 6$ , collected at 294 K, for both the samples, is employed for ample charge density studies.

### 3. Structure refinement, general structure properties and Debye-Waller factors

The raw structure factors, obtained from the synchrotron X-ray data of CoF<sub>2</sub> and NiF<sub>2</sub> crystals are refined by using anharmonic model of a standard least squares full matrix method. This method includes the prior corrections for absorption [63], scale, harmonic and anharmonic thermal parameters and extinction effects using a Zachariasen model [64] and for Thermal Diffuse Scattering parameters (TDS). In this technique, the quantity to be reduced is,

$$D = \sum_{hkl} W_{hkl} (|F_o| - |F_c|)^2$$

Here the weight which is assigned to an observation is  $W_{hkl}$  and the

**Table 4**  
Topological properties at the (3,-1) Bond Critical Points.

Oxidation state	Molecules	Bond	Symmetry	MEM			Multipole	Tsirelson's classification of BCP, $\rho$ ( $e/\text{\AA}^3$ )		
				d ( $\text{\AA}$ )	$d_1$ ( $\text{\AA}$ )	$d_2$ ( $\text{\AA}$ )	d ( $\text{\AA}$ )	Ionic interactions	Intermediate interactions	Polar covalent interactions
+1	LiF [26]	Li-F	-	2.0100	0.9300	1.2800	-	0.0673	-	-
	NaF [26]	Ni-F	-	2.3100	0.9000	1.4100	-	0.0030	-	-
+2	CoF <sub>2</sub>	Co-F	Co - (-y+1/2, x+1/2, z+1/2)	2.0562	0.8130	1.2432	2.0556	-	0.6856	-
			F - (-x, -y, -z) Fig. 4(a)							
	Co - (-y+1/2, x+1/2, z+1/2)	2.0161	0.7762	1.2399	2.0158	-	0.4367	-		
	F - (y+1/2, -x+1/2, -z+1/2) Fig. 4(c)									
NiF <sub>2</sub>	Ni-F	Ni - (-y+1/2, x+1/2, z+1/2)	2.0051	0.9875	1.0176	2.0046	-	0.4229	-	
		F - (-x, -y, -z) Fig. 4(b)								
		Ni - (-y+1/2, x+1/2, z+1/2)	1.9833	0.8368	1.1465	1.9828	-	0.5433	-	
		F - (y+1/2, -x+1/2, -z+1/2) Fig. 4(d)								
+3	GaF <sub>3</sub> [27]	Ga-F	-	1.8994	0.9086	0.9908	1.8990	-	0.7190	-
	VF <sub>3</sub> [27]	V-F	-	1.9829	0.8725	1.1104	1.9832	-	0.6191	-

observed and calculated structure factors are  $F_O$  and  $F_C$  respectively.

As a result of structure refinement, a best possible fit between the observed and calculated structure factors were realized. The geometrical results thus achieved, given in Table 1, are in admirable agreement with other literature values reported already [32–34,37,41,47,48,50–52,56]. The isotropic and anisotropic parameters of Co, Ni and F atoms are compared with the reported values in Table 2.

Several works including our own works [15,27,65–67] have evidenced the universal truth that the vibration of the heavier atoms will be less when compared to that of the lighter atoms. In the present work also, from the Debye-Waller factors presented in Tables 1 and 2, it is clear that in both the systems, the lighter fluorine ( $Z(F) = 9$ ) atom has large thermal vibrational amplitude compared to the heavier constituent atoms, Co and Ni. It is experimentally observed that the increasing trend of vibration is in the order: Ni < Co < F. A keen observation on the  $B_{iso}$  values of F atom in the two molecules has pointed out that the vibration of fluorine atom is larger in CoF<sub>2</sub> than in NiF<sub>2</sub> with a difference of 0.09253  $\text{\AA}^2$ . This indicates that nickel difluoride has slightly larger binding force than cobalt difluoride.

The very low reliability indices (1.81% for cobalt fluoride and 1.25% for nickel fluoride), in Table 1, indicate the precision of the data and successful refinements and this implies that the data is suitable for charge density studies.

#### 4. Data analysis

To do away with experimental noise in the data, Bayesian statistical analysis [15] was performed. Further, as the electron density studies demand accurate structure factors, error analysis is done as a testing ground to authorize the data quality. Hence the two yardstick tests of error analysis: (i) histograms of the number of reflections against the function  $[F_{MEM}(k)-F_{Obs}(k)]/\sigma(k)$  and (ii) error maps in the reciprocal lattice space, are plotted and given as Fig. 2. In the histogram, the set of reflections with least  $[F_{MEM}(k)-F_{Obs}(k)]/\sigma(k)$  are maximum and the values adhere to a natural Gaussian distribution (Fig. 2(a) and (b)). Additionally, the error function distributed shows the spread of errors within a minimum value of  $\pm 2$  (Fig. 2(c) and (d)). Thus our analysis fall within their error bounds disclosing the worth of the data. Thus after validating the quality of the data being good, the charge density study was proceeded.

#### 5. MEM refinements and reliability indices

A precise mapping of electron density distribution is acquired by

using Maximum entropy method (MEM), proposed by Collins [68], which serves as a faithful statistical and probabilistic approach of charge density. Hence, the refined structure factors are further used for MEM analysis. At first, the unit cells of CoF<sub>2</sub> and NiF<sub>2</sub> systems are divided so as to contain  $95 \times 95 \times 64$  pixels in concurrence with their ratio of the dimensions of the cell along the three crystallographic axes. According to the method proposed by Sakata and Sato [69], to compute the charge density, the principle is that the most probable density is the one which simultaneously maximizes the entropy in an iterative cycle in the  $i^{\text{th}}$  pixel in a unit cell, in terms of the assumed uniform prior density at that pixel, fulfilling the constraint of the normalization of the density,

$$C = \frac{1}{N} \sum_k \frac{|F_{obs}(k) - F_{cal}(k)|^2}{\sigma^2}$$

and it fits the diffraction data. Thus the electron density is,

$$\rho_{MEM}(r_i) = \tau(r_i) \exp \left[ \left( \frac{\lambda F_{000}}{N} \right) \sum [1/\sigma(k)]^2 |F_{obs}(k) - F_{cal}(k)| \exp(-2\pi j k \cdot r) \right]$$

Here  $N$ ,  $F_{obs}(k)$ ,  $F_{cal}(k)$  and  $\sigma$  stand for the number of reflections, observed and calculated structure factors and standard deviation correspondingly,  $\tau(r_i)$  is the prior electron density and  $F_{000}$  is the number of electrons in the unit cell. For computation facility, the software PRIMA [70,71], which implements this method is used for the present study and the results are given in Table 3.

At each of the pixels, the prior charge density is fixed uniformly as  $F_{000}/a^2c = 1.2839 e/\text{\AA}^3$  for CoF<sub>2</sub> and  $1.3982 e/\text{\AA}^3$  for NiF<sub>2</sub>, as the total charges in the unit cell of cobalt fluoride is 90.00 and that in nickel fluoride is 92.00. The convergence criterion  $C$ , tend to 1 after 174 and 192 iterative cycles for CoF<sub>2</sub> and NiF<sub>2</sub> respectively. Thus the number of refinement cycles is slightly higher for the latter than the former, probably due to the slightly more number of electrons in the unit cell in the latter, which has been divided into the same number of pixels in both the systems. The low reliability index values as established as 1.26% for CoF<sub>2</sub> and 1.07% for NiF<sub>2</sub> reveal the high quality nature of the two available data sets.

Table 3 shows that the total charges in one unit cell of NiF<sub>2</sub> is slightly more than that in one unit cell of CoF<sub>2</sub>, but the volume of the unit cell of CoF<sub>2</sub>, as shown in Table 1, is less than that of NiF<sub>2</sub>. This discloses that the unit cell of nickel difluoride is packed more closely than that of cobalt difluoride.

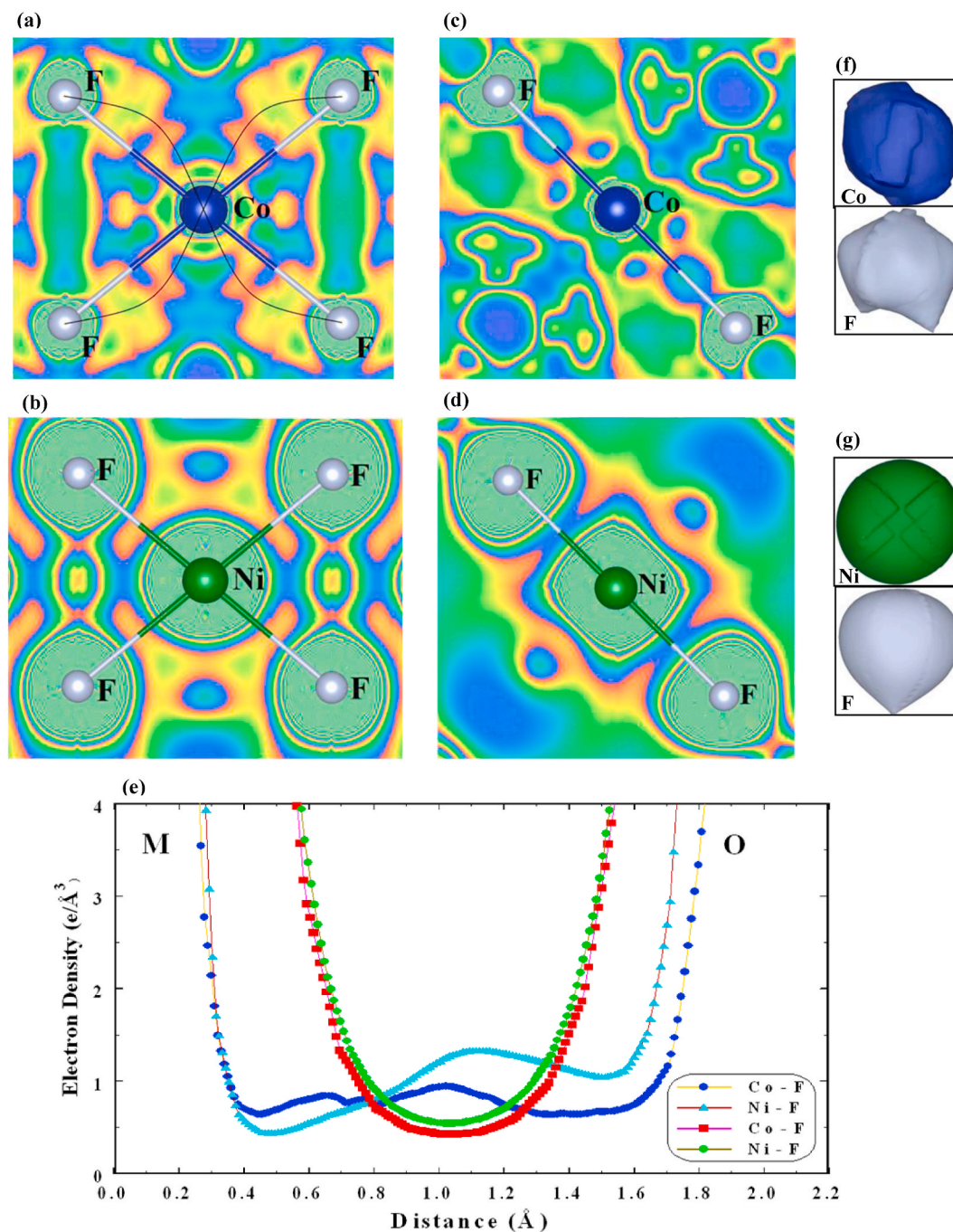


Fig. 4. Two-dimensional electron density maps of M – F bonds in (a) and (b) CoF<sub>2</sub> and (c) and (d) NiF<sub>2</sub>. (e) One dimensional charge density profiles of M – F bonds. Atomic basins of (f) CoF<sub>2</sub> and (g) NiF<sub>2</sub>.

## 6. Multipole and Kappa refinements and deformation density maps

The more consistent and adaptable refinement technique which provides an analytical distribution of charge density, called the multipole model refinement, is implemented to the subjects of our study, to understand the complicate details of the charge related parameters including the contraction/expansion of atoms in the systems. In accordance with Hansen and Coppens [72] model, the multipole density,

$$\rho(r) = \sum_k^{\text{atoms}} \rho(r - r_k - u) \otimes t_k(u),$$

where  $t_k(u)$  means the Gaussian term and the symbol  $\otimes$  shows the convolution, is the superposition of harmonically vibrating aspherical atomic density distribution and every atomic density defined as,

$$\rho(r) = P_c \rho_{\text{core}}(r) + P_v \kappa^3 \rho_{\text{valence}}(\kappa r) + \sum_{l=0}^4 \kappa'^3 R_l(\kappa' r) + \sum_{m=-1}^l P_{lm} Y_{lm} \left( \frac{\vec{r}}{r} \right)$$

where  $P_c$ ,  $P_v$  and  $P_{lm}$  indicate the population coefficients. The Slater type radial function,  $R_l(\kappa' r)$ , is a sequence expansion in real spherical harmonic functions through fourth order  $Y_{lm}$ .  $\rho_{\text{core}}$  and  $\rho_{\text{valence}}$  parameters can be built by means of canonical Hartree – Fock atomic orbitals of the free atoms normalized to one electron and permitting the valence function to expand and contract by adjusting the variable parameters  $\kappa$

**Table 5**  
**Bond lengths and bond angles.**

References		Bond lengths (M – F) (Å)		Bond angles (F – M – F) (degrees)	
		CoF <sub>2</sub>	NiF <sub>2</sub>	CoF <sub>2</sub>	NiF <sub>2</sub>
Present work	MEM	2.0562 (0)	2.0051 (5)	90.00 (6)	90.00 (14)
		2.0161 (0)	1.9833 (7)	180.00 (6)	180.00 (17)
	Multipole	2.0556 (8)	2.0046 (3)	90.00 (0)	90.00 (1)
		2.0158 (3)	1.9828 (5)	180.00 (0)	180.00 (5)
[34]		2.0570 (4)	-	101.27 (5)	80.13 (13)
[37]		2.0149 (6)	-	78.73 (5)	80.13 (5)
[41]		2.05 ± 0.02	2.04 ± 0.02	90	90
[50]		2.04 ± 0.01	1.98 ± 0.01	102	99.6
		2.058 (1)	2.011 (1)	78	80.4
		2.014 (1)	1.997 (1)	-	-

and  $\kappa'$ .

In the present work, the software JANA 2006 [73] is used for multipole refinement of core, valence and pseudo-atomic electron occupancies  $P_{lm}$ . According to Hansen and Coppens [72], the neutral atom wave functions are extorted from Clementi tables [74] and the Slater type radial functions are used with  $n_l = 4\ 4\ 6\ 8$  for Co/Ni and  $n_l = 2\ 2\ 2\ 3$  for F for  $l \leq 4$ . The core charges are taken as Ar for Co/Ni and He for F atom during refinement and for all the three atoms, the valence expansion/contraction parameter ( $\kappa$ ) is refined in the two data sets. The results of the multipole refinement are presented as Table 3. The refined parameters,  $\kappa$  and  $\kappa'$  are the indications of expansion and contraction of atoms by exposing its values as greater than unity or less than unity correspondingly. Relevant to this argument, the  $\kappa$  values of metal atoms in the table (1.0251 for Co and 1.0536 for Ni) show the signs of contraction whereas the same of ligand atoms reveal the expansion nature as its  $\kappa$  values are less than 1. These effects replicate in the values of core ( $P_c$ ) and valance ( $P_v$ ) charges of the individual atoms, i.e., the sum of  $P_c$  and  $P_v$  values of Co and Ni are 26.1330 and 27.6953 respectively and as these values are less than its actual Z values, confirms the contraction of both the atoms in their respective molecule. Similarly, the sum of  $P_c$  and  $P_v$  values of F atom in CoF<sub>2</sub> is 9.4438 and in NiF<sub>2</sub> is 9.3854. This confirms the expansion of atoms, since these values are greater than the actual Z value of fluorine atom in both the systems. Hence the two systems exhibit the same behavior in the course of expansion/contraction while bonding. However, since the shape of the valence charges is completely aspherical,  $\kappa'$  would be very difficult to refine in both cobalt fluoride and nickel fluoride.

Deformation density maps are drawn (Fig. 3) to notice the effect of temperature on the charge distribution, in which the density of deformation is,

$$\Delta\rho_{\text{multipole-deformation}}(\vec{r}) = \frac{1}{V} \sum \left[ F(\vec{h})_{\text{multipole}} - F(\vec{h})_{\text{spherical-atom}} \right] \exp \left[ -2\pi i (\vec{h} \cdot \vec{r}) \right]$$

where  $F_{\text{multipole}}$  denotes the Fourier transform of the multipole electron density with or without convolution of thermal contribution. The fourier components are concluded at the experiment resolution. The difference

fourier maps of CoF<sub>2</sub> and NiF<sub>2</sub> shown as Fig. 3(a) and (b) respectively, indicate less noise and background density, once again confirming the better quality of the data. In addition to this, the dynamic deformation maps (Fig. 3(c) and (d)) point out the convoluted form while the static deformation maps in Fig. 3(e) and (f) indicate the deconvoluted form of thermal contribution in cobalt difluoride and nickel difluoride. The maps expose the less deformation of atoms. The lone pair electrons of fluorine atoms are clearly visible in the figures. Amusingly, perceiving the DMD and SMD figures, the lone pair orbitals of F atoms seem to interact with each other.

## 7. Topological analysis of charge density and characterization of bonding

To provide a more faithful documentation of the concept of atoms, bonds and structure, the topology of electron density, facilitated by the theory of “Atoms In Molecules (AIM)”, developed by Bader [75] (as quoted as “two atoms are bonded if they are connected by a line of maximum electron density called a bond path, on which lies a bond critical point (BCP) where  $\vec{\nabla}\rho(r_{BCP}) = 0$ , and the critical points are the characteristics of the bond existing between the atoms”), is analysed for the two subjects of our study. Hence, as discussed earlier, bond critical point (BCP) search and the calculation of the properties of charge density at these points are performed by both MEM and multipole methods. By maximum entropy method, the valence charge density is obtained along the bond path through high resolution (0.08 eÅ<sup>-3</sup>/pixel) electron density distribution maps in three, two and one dimensions (Fig. 1(b) and (c) and 4) using the software VESTA [75]. By means of Newton-Raphson method, the (3,-1) bond critical points are searched in the places between every pair of neighboring nuclei. The bond lengths and angles and the amount of intermediate charges, measured in these two analyses are tabulated as Tables 4 and 5. In Table 4, d, d<sub>1</sub> and d<sub>2</sub> signify the M atom – F atom, M atom – CP (Critical Point) and CP – F atom distances respectively. For +1 and +3 oxidation states of metal, the charge density at the bond critical points of the monofluorides of lithium and sodium [26] and the trifluorides of gallium and vanadium [27] respectively, are also included in the table. The present obtained values are compared with the reported ones in Table 5. The results obtained from both multipole and MEM analyses matches very well for the two compounds.

Before discussing the nature of bonds it is desirable to stipulate the logic in which the terms ionic and covalent is used. The AIM theory, proposed by Bader [76], uses charge density as its initial point and offers a powerful tool for categorizing the bonding state. According to Bader [76] and Tserelson [77], the presence and classification of a chemical bond are based on the electron density at the saddle point (Bond Critical Point, BCP) between two nuclei and on the values of its associated length of the bond. As a consequent, a low value of  $\rho(bcp)$  less than 0.3 e/Å<sup>3</sup>, combined with a long bond is typical for closed - electron interactions and the value of  $\rho(bcp)$  greater than 0.3 e/Å<sup>3</sup>, but less than 1 e/Å<sup>3</sup>, is categorized as intermediate interactions whereas, unshared - electron interactions is characterized by  $1 < \rho(bcp) < 2$  e/Å<sup>3</sup> and short bond length [60,67,77–79].

In this regime, the physical evidence of such effects in terms of the electron density distribution is shown by sketching three dimensional MEM maps for cobalt fluoride and nickel fluoride in ball and stick model of structure with isosurface level of 0.8 e/Å<sup>3</sup> (Fig. 1(b) and (c)). In the maps, the shapes of constituent atoms and the bonds between them are clearly revealed. The most remarkable feature observed in the maps is, depending on the symmetry, the atoms display diverse bonding nature in both the fluorides.

For a more clear visualization of density in the bonding regions and to categorize the bonds in difluorides, 2 – D and 1 – D MEM maps are plotted (Fig. 4). Moreover, in this work, the 2 – D maps are plotted in RGB (Red Green Blue) scale, in which the red shade in the saddle area

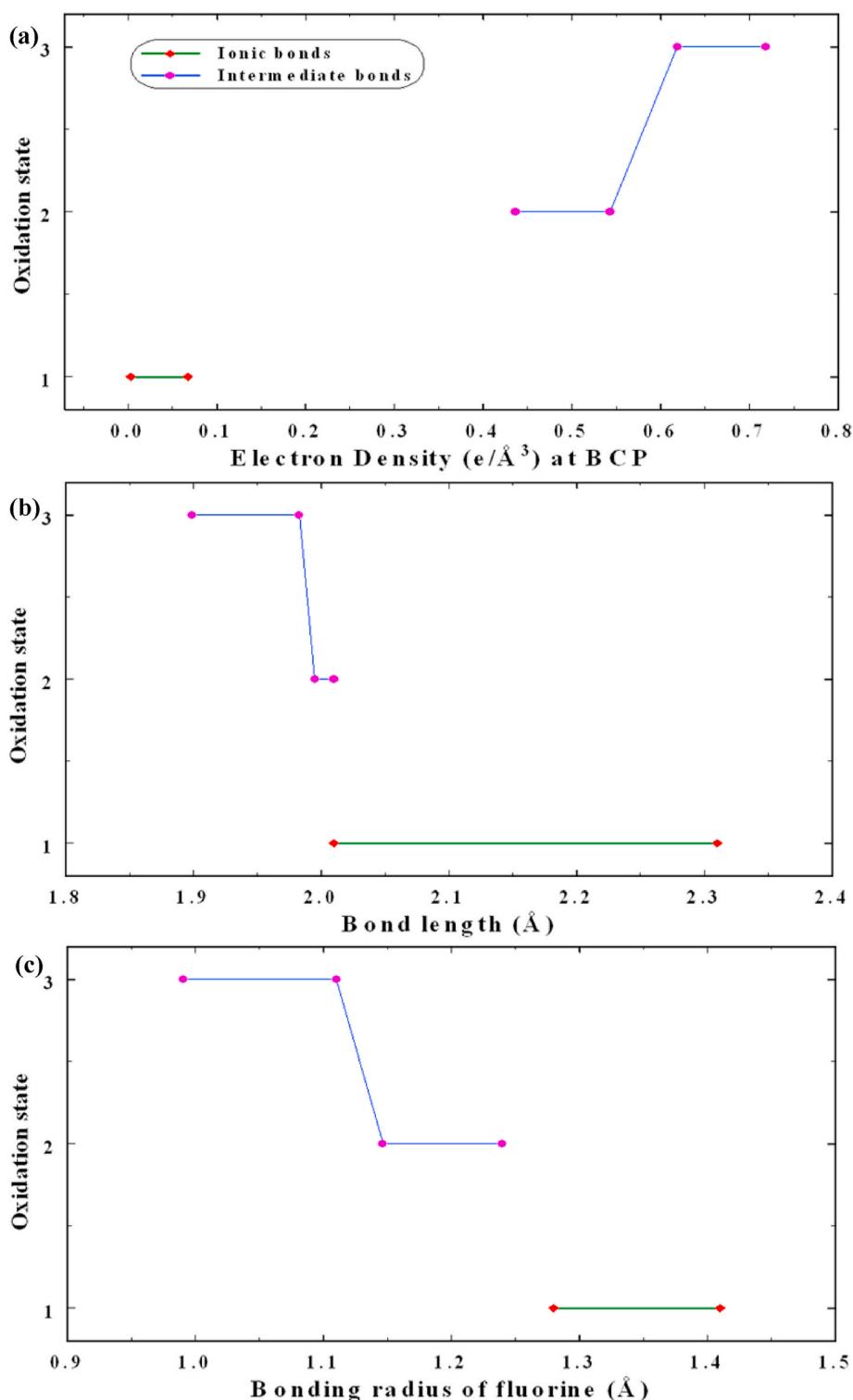


Fig. 5. Oxidation state of metal versus (a) electron density at bcp, (b) bond length and (c) bonding radius of fluorine.

specifies high density regions whereas the blue shade indicates the low density regions. The curved bond paths are also shown in the maps. The 3 – D, 2 – D and 1 – D maps and Tables 5 and 6 substantiate the two dissimilar bond lengths,  $d_1$  and  $d_2$ , and the electron density at BCP exhibited by the fluorides of cobalt and nickel. The mid-bond density between cobalt atom at  $(-y+1/2, x+1/2, z+1/2)$  and fluorine atom at  $(-x, -y, -z)$  is  $0.6856 e/\text{\AA}^3$  (Table 4) and these comparatively high density regions are signified by red saddles in Fig. 4(a), whereas the mid-bond density between the nickel and fluorine atom at the same symmetries

is  $0.4229 e/\text{\AA}^3$  and the well resolved Ni atoms in Fig. 4(b) indicate the low density regions. In contrast, the same Co atom, when it bonds to F atom at  $(y+1/2, -x+1/2, -z+1/2)$ , results in a low value of  $\rho$  at CP ( $0.4367 e/\text{\AA}^3$ ) while the same in case of nickel fluoride shows a comparatively high  $\rho$  value of  $0.5433 e/\text{\AA}^3$ . The highly resolved electron clouds in Fig. 4(c) and blue saddles in Fig. 4(d) show the signs of the above argument. The one dimensional MEM map (Fig. 4(e)) also imitate these outcomes. In the figure, the profiles of bonds, having relatively high density at CP, of  $\text{CoF}_2$  and  $\text{NiF}_2$  have elongated saddles with Non-

Nuclear Maxima (NNM). Moreover, analogous to the dynamic and static multipole density maps, the MEM maps also show the interactions between the lone pair electron orbitals of ligand atoms in the two compounds (Fig. 4(a) and (b)).

In contrast to the arguments of pure ionic nature of bonding in CoF<sub>2</sub> and NiF<sub>2</sub>, by Nicholas J.O' Toole et al. [34], Palmer et al. [48], Jauch et al. [51], and Brown et al. [56], all these well analysed data reveal the fact that the interactions between the metal and ligand atom in both the difluorides, as classified by Tsierson [77], are intermediate, since the density of charges at BCP are greater than 0.3 e/Å<sup>3</sup> and less than 1 e/Å<sup>3</sup>. Indeed, as viewed by Costa et al. [50], the elongated saddles with relatively high  $\rho$  values in certain bonds of both the compounds emphasize covalent effects in bonding. For further lucid interpretation, the shortest bond in each molecule is taken in to account, in view of the fact that it is the strongest and best possible bond with a perfect geometrical arrangement of atoms. Table 4 stresses the point that the electron density at the critical point of the shortest bond (2.0161 Å) in CoF<sub>2</sub> (0.4367 e/Å<sup>3</sup>) is less than that in NiF<sub>2</sub> (0.5433 e/Å<sup>3</sup>). This confirms that cobalt difluoride has more ionic character than nickel difluoride. The ionic and covalent radii of Co are 0.65 Å and 1.16 Å and that of Ni are 0.69 Å and 1.15 Å respectively. Though the value of  $d_1$  in both CoF<sub>2</sub> (0.7762 Å) and NiF<sub>2</sub> (0.8368 Å) lies between those of  $r_i$  and  $r_c$  of the corresponding atoms, in case of nickel fluoride, as the  $d_1$  value approaches the  $r_c$  value of metal atom, the latter has slightly more covalent nature of bonding than the former.

The two dimensional MEM maps of cobalt difluoride and nickel difluoride clearly exhibit the spherical and aspherical nature of atoms, while bonding. Hence, for the close exploration of this asphericity, true valence charge density figures are drawn by recognizing zero flux surface (ZFS) at all directions which encapsulates the atomic basins (i.e., regions of space traversed by trajectories of the density gradient termination at a given nucleus which is enclosed inside a zero charge density flux surface,  $\vec{\nabla}\rho \cdot \vec{n}$ , where  $\vec{n}$  is the unit vector of surface) (Fig. 4(f) and (g)). The figures overtly divulge the fact that the atomic basins of the atoms are not influenced by the symmetries and bonding natures of the atoms. Except the basin of Ni atom, which is close to spherical shape, as viewed by Ian Bytheway [80], the figures of the basins of the transition metal (Co) atom and polarized ligand atoms show asphericity.

The second main object of this search, i.e. to compare these difluorides with monofluorides and trifluorides, a complete map of the oxidation state of the metal versus electron density at bcp, bond length and bonding radius of fluorine (Fig. 5) is established. At +1 oxidation state of metals, the low  $\rho$  values (less than 0.3 e/Å<sup>3</sup>) and high  $d$  values in Fig. 5(a) and (b) indicate that the bonds are predominantly ionic and very weak. The bonding radius of fluorine is also high (Fig. 5(c)). The increase in oxidation state of metal cations, increases the importance of polar covalent character in bonds which is signified by the raise in the electron density at the critical point. Hence, from +2 oxidation state of cation, interactions between the metal and ligand atoms are intermediate and as a result, the strength of the bonds also increases, with a decrease in bonding radius of fluorine. Even though the interactions in both the difluorides and trifluorides are intermediate, the electron density at BCP of trifluorides is relatively high with small and strong bonds and a very low bonding radius of fluorine. Thus this graph is the vital step to serve the intention of this paper, as it demonstrates the degree of the involvement of covalency in binary fluorides with respect to oxidation state of metal cations.

Hence reconciling our systematic charge density study on the difluorides of cobalt and nickel, it is concluded that NiF<sub>2</sub> is more rigid and CoF<sub>2</sub> is fragile. Perchance, the dense packing of atoms in the unit cell of the former and the slackly packing nature of the latter forms the root of the above proposed argument. An important result emerging from the two complimentary techniques (MEM and multipole) of electron density estimation is the evidence for intermediate type of bonding in both the

systems. In addition to this, between these two molecules, it is experimentally found that NiF<sub>2</sub> contains more covalent character than CoF<sub>2</sub>. Our conclusions from the investigation of fluorine bonding with respect to the ascending order of the oxidation state of metal cations is that, at low oxidation states (+1) the ionic character of bonding predominates in binary fluorides and as the oxidation state increases, gradually, the intermediate interactions are found to be taking up. Consequently, there is a small but increasing involvement of covalent bonding and this contribution follows the trend:  $Co^{2+} < Ni^{2+} < Ga^{3+} < V^{3+}$ .

## 8. Conclusion

The present charge density work of the two transition metal difluorides has provided a more complete picture of the electronic structure of the material, and ample informations on the nature of bonding between its constituent atoms. Charge densities along different bonding planes, validated qualitatively as well as quantitatively, clearly reveals that these systems exhibit intermediate type of bonding and NiF<sub>2</sub> has more covalent nature of bonding than CoF<sub>2</sub>. Moreover, nickel difluoride is a hard molecule than cobalt difluoride. In addition to this, our present work collects into one place the pertinent pieces of information about the bonding properties of certain binary metal fluorides. At very low oxidation state of metals, fluorides are purely ionic and as the oxidation state ascends, they exhibit intermediate interactions with a gradual increase in covalent mixing. Thus a satisfactory correlation between fluorides with different oxidation state of cations is established. Same sort of findings in fluoride based materials will open up the possibility of tuning the structural and electronic properties of fluorides, which is necessary for technological application and in turn, lead to an era where fluoride devices will become a feasible and integral part of many exotic devices.

## Declaration of competing interest

The authors declare that they have no known competing financial interests or personal relationships that could have appeared to influence the work reported in this paper.

## References

- [1] Bo-Huei Liao, Chien-Nan Hsiao, Cheng-Chung Lee, Aluminium oxyfluoride films for deep ultraviolet optics deposited by a combined HIPIMS/CFUBMS deposition technique, *Opt. Mater. Express* 6 (No. 5) (2016) 1506–1512.
- [2] T. Dayaldas, Meshri, "Industrial Applications of Inorganic Fluorides", Elsevier Science S.A., 2000.
- [3] Neil Bartlett, *Introductory Remarks*, Elsevier Science S.A., 2000.
- [4] Jean-Luc Adam, *Optical Properties and Applications of Fluoride Glasses*, Elsevier Science S.A., 2000.
- [5] Kiyoshi Kanamura, *Fluorine Compounds in Battery Applications*, Elsevier Science S.A., 2000.
- [6] John Emsley, "Nature's Building Blocks: an A-Z Guide to the Elements", second ed., Oxford University Press, New York, 2011.
- [7] G. Glenn, Amatucci, Nathalie Pereira, "Fluoride based electrode materials for advanced energy storage devices", *J. Flour. Chem.* 128 (2007) 243–262.
- [8] J.L.G. Fierro, *Metal Oxides: Chemistry and Applications*, CRC Press, 2005.
- [9] Hari Singh Nalwa, *Handbook of Surfaces and Interfaces of Materials, Five-Volume Set*, Academic Press, 2001.
- [10] P.D.C. King, T.D. Veal, A. Scliefe, J. Zuniga-Perez, B. Martel, P.H. Jefferson, F. Fuchs, V. Munoz-Sanjose, F. Bechstedt, C.F. McConville, Valence-band electronic structure of CdO, ZnO, and MgO from x-ray photoemission spectroscopy and quasi-particle-corrected density-functional theory calculations, *Phys. Rev. B* 79 (2009) 205205.
- [11] M. Veronica Ganduglia-Pirovano, Alexander Hofmann, Joachim Sauer, Oxygen vacancies in transition metal and rare earth oxides: current state of understanding and remaining challenges, *Surf. Sci. Rep.* 62 (2007) 219–270.
- [12] C.N.R. Rao, H. Transition metal oxides (including cuprate superconductors), *Annu. Rev. Phys. Chem.* 40 (1989) 291–326.
- [13] S.K. Deb, Physical properties of a transition metal oxide: optical and photoelectronic properties of single crystal and thin film molybdenum trioxide, *Proc. Roy. Soc. A* 304 (1968) 211–231.
- [14] SivachandranBalendran SumeetWalia, Hussein Nili, Serge Zhuiykov, Rosegarten Gary, Qing Hua Wang, SharathSriram MadhuBhaskaran, Michael S. Strano, KouroushKalantar-zadeh, "Transition metal oxides – thermoelectric properties", *Prog. Mater. Sci.* 58 (8) (2013) 1443–1489.

- [15] K. Sujatha, S. Israel, C. Anzline, X-ray derived experimental charge density distribution in two isostructural oxyfluorotellurates,  $\text{FeTeO}_3\text{F}$  and  $\text{GaTeO}_3\text{F}$ , *Physica B* 579 (2020) 1–12, 411896.
- [16] A. Trueba, P. Garcia-Fernandez, J.M. Garcia-Lastra, J.A. Aramburu, M.T. Barriuso, M. Moreno, Transition metal impurities in fluorides: role of electronic structure of fluorine on spectroscopic properties", *J. Fluor. Chem.* 132 (2011) 747–754.
- [17] Linus Pauling, The nature of the chemical bond. IV. The energy of single bonds and the relative electronegativity of atoms, *J. Am. Chem. Soc.* 54 (1932) 3570–3582.
- [18] John H. Holloway, Eric G. Hope, Novel synthesis using inorganic fluorides, *J. Fluor. Chem.* 76 (1996) 209–212.
- [19] Karel Lutar, Horst Borrmann, Marc Leblanc, "Recent Developments in the Synthesis of Inorganic Fluorides", Elsevier Science S.A., 2000.
- [20] R. Andrew, Barron, "Compounds of Fluorine", OpenStax-CNX module: m33815, 2010, pp. 1–4.
- [21] A.J. Edwards, Solid-state structures of the binary fluorides of the transition metals, *Adv. Inorg. Chem.* 27 (1983) 83–112.
- [22] M. John, Winfield, "Transition metal fluorides", *J. Fluor. Chem.* 33 (1986) 159–178.
- [23] Sophie L. Benjamin, William Levason, Gillian Reid, Medium and high oxidation state metal/non-metal fluoride and oxide-fluoride complexes with neutral donor ligands, *Chem. Soc. Rev.* 42 (2013) 1460–1499.
- [24] Wolfgang W. Dukat, John H. Holloway, Eric G. Hope, Matthias R. Rieland, Paul J. Townson, High oxidation state binary transition metal fluorides as selective fluorinating agents, *J. Chem. Soc., Chem. Commun.* 18 (1993) 1429–1430.
- [25] A. Higelin, S. Riedel, "High oxidation states in transition metal fluorides", Modern synthesis processes and reactivity of fluorinated compounds, *Prog. Fluor. Sci.* (2017) 561–586.
- [26] S. Israel, R. Saravanan, N. Srinivasan, R.K. Rajaram, High resolution electron density mapping for  $\text{LiF}$  and  $\text{NaF}$  by maximum entropy method (MEM)", *J. Phys. Chem. Solid.* 64 (2003) 43–49.
- [27] K. Sujatha, S. Israel, C. Anzline, R. Niranjana Devi, R.A.J.R. Sheeba, X-ray derived experimental charge density distribution in  $\text{GaF}_3$  and  $\text{VF}_3$  solid systems, *Physica B* 496 (2016) 74–81.
- [28] S. Tibor, Koritsanszky, Philip Coppens, "chemical applications of X-ray charge-density analysis", *Chem. Rev.* 101 (2001) 1583–1627.
- [29] G.U. Kulkarni, R.S. Gopalan, C.N.R. Rao, Experimental and theoretical electronic charge densities in molecular crystals, *J. Mol. Struct.* 500 (2000) 339–362.
- [30] R. Saravanan, M. Prema Rani, Metal and Alloy Bonding: an Experimental Analysis, Springer-Verlag London Limited, 2012.
- [31] J. Jimenez-Mier, P. Olalde-Velasco, P. DeLa Mora, W.-L. Yang, J. Denlinger, Atomic multiplet and charge transfer effects in the resonant inelastic X-ray scattering (RIXS) spectra at the Nickel  $L_{2,3}$  edge of  $\text{NiF}_2$ , *J. Nucl. Phys. Mater. Sci. Rad. Appl.* 5 (No-1) (2017) 1–13.
- [32] Cihan kurkcü, Ziya Merdan, Hulya Ozturk, "Pressure – induced phase transitions and structural properties of  $\text{CoF}_2$ : an ab – initio molecular dynamics study", *Solid State Commun.* 231 – 232 (2016) 17–25.
- [33] S. Arumugam, P. Sivaprakash, Ambesh Dixit, Rajneesh Chaurasiya, L. Govindaraj, M. Sathiskumar, Souvik Chatterjee, R. Suryanarayanan, Complex magnetic structure and magneto-capacitance response in a non-oxide  $\text{NiF}_2$  system, *Sci. Rep.* 9 (2019) 1–8.
- [34] Nicholas J.O' Toole, Victor A. Streltsov, Synchrotron X-ray analysis of the electron density in  $\text{CoF}_2$  and  $\text{ZnF}_2$ , *Acta Crystallogr. Sect. B Struct. Sci.* B57 (2001) 128–135.
- [35] Giancarlo Cappellini, Jurgen Furthmüller, Emiliano Cadelano, Friedhelm Bechstedt, Electronic and optical properties of cadmium fluoride: the role of many-body effects, *Phys. Rev. B* 87 (2013) 1–9.
- [36] P. Fischer, D. Schwarzenbach, H.M. Rietveld, Crystal and magnetic structure of silver difluoride: I. Determination of the  $\text{AgF}_2$  structure, *J. Phys. Chem. Solid.* 32 (Issue 3) (1971) 543–550.
- [37] M. Balkanski, P. Moch, G. Parisot, Infrared lattice-vibration spectra in  $\text{NiF}_2$ ,  $\text{CoF}_2$  and  $\text{FeF}_2$ , *J. Chem. Phys.* 44 (Number 3) (1966) 940–944.
- [38] Hena Das, Sudipta Kanungo, T. Saha-Dasgupta, First-principles study of magnetoelastic effect in the difluoride compounds  $\text{MF}_2$  ( $M = \text{Mn, Fe, Co, Ni}$ ), *Phys. Rev. B* 86 (2012) 054422–054431.
- [39] D.J. Lockwood, M.G. Cottam, Magneto-optic coupling coefficients for one- and two-magnon Raman scattering in rutile-structure antiferromagnets  $\text{FeF}_2$ ,  $\text{MnF}_2$ ,  $\text{CoF}_2$  and  $\text{NiF}_2$ , *Low Temp. Phys.* 38 (Number 7) (2012) 549–558.
- [40] Kei-ichiro Murai, Yohei Suzuki, Toshihiro Moriga, Akira Yoshiasa, "EXAFS and XPS study of rutile-type difluorides of first-row transition metals", X-ray absorption fine structure, *AIP Conf. Proc.* 882 (2007) 1–3.
- [41] J.W. Stout, Stanley A. Reed, The crystal structure of  $\text{MnF}_2$ ,  $\text{FeF}_2$ ,  $\text{CoF}_2$ ,  $\text{NiF}_2$  and  $\text{ZnF}_2$ , *Cryst. Struct. Anhyd. Fluorides* 76 (1954) 5279–5281.
- [42] A.J. Edwards, Solid-state structures of the binary fluorides of the transition metals, *Adv. Inorg. Chem.* 27 (1983) 83–112.
- [43] R.A. Erickson, Neutron diffraction studies of antiferromagnetism in Manganous fluoride and some isomorphous compounds, *Phys. Rev.* 90 (No. 5) (1953) 779–785.
- [44] A.S. Borovik-Romanov, Piezomagnetism in the antiferromagnetic fluorides of cobalt and manganese, *Sov. Phys. - JETP* 11 (Number 4) (1960) 786–793.
- [45] R. De Renzi, G. Guidi, P. Podini, R. Tedeschi, C. Bucci, S.F.J. Cox, Magnetic properties of  $\text{MnF}_2$  and  $\text{CoF}_2$  determined by implanted positive muons. I. Localization studies, *Phys. Rev. B* 30 (Number 1) (1984) 186–196.
- [46] Tapan Chatterji, Gail N. Iles, Bachir Ouladdial, Thomas C. Hansen, Magnetoelastic effect in  $\text{MF}_2$  ( $M = \text{Mn, Fe, Ni}$ ) investigated by neutron powder diffraction, *J. Phys. Condens. Matter* 22 (2010) 1–11.
- [47] W. Jauch, A. Palmer, Single-crystal pulsed neutron diffraction from  $\text{NiF}_2$  and  $\text{FeF}_2$ : the effect of magnetic order on the fluorine positions, *Acta Crystallogr. B* B49 (1993) 984–987.
- [48] A. Palmer, W. Jauch, Charge-density analyses of the antiferromagnets  $\text{NiF}_2$  and  $\text{FeF}_2$  by means of  $\gamma$ -ray diffraction, *Phys. Rev. B* 48 (Number 14) (1993) 10304–10310.
- [49] Munnangi Anji Reddy, Maximilian Fichtner, "Fluoride Cathodes for Secondary Batteries", Book - "Advanced Fluoride-Based Materials for Energy Conversion", Elsevier, 2015.
- [50] M.M.R.Costa, J.A.Paixao, M.J.M.De Almeida and L.C.R.Andrade, "Charge densities of two rutile structures:  $\text{NiF}_2$  and  $\text{CoF}_2$ ", *Acta Crystallogr. B*, B49, 591 – 599.
- [51] W. Jauch, M. Reehuis, A.J. Schultz,  $\gamma$ -ray and neutron diffraction studies of  $\text{CoF}_2$ : magnetostriction, electron density and magnetic moments, *Acta Cryst. A Found. Crystall.* A60 (2004) 51–57.
- [52] J.A. Barreda-Argueso, S. Lopez-Moreno, M.N. Sanz-Ortiz, F. Aguado, R. Valiente, J. Gonzalez, F. Rodriguez, A.H. Romero, A. Munoz, L. Nataf, F. Baudelet, Pressure – induced phase transition sequence in  $\text{CoF}_2$ : an experimental and first-principles study on the crystal, vibrational and electronic properties, *Phys. Rev. B* 88 (2013) 214108–214115.
- [53] Y. Shapira, Paramagnetic to antiferromagnetic phase boundary of  $\text{CoF}_2$  from ultrasonic measurements, *Journal de physique archives* 32 (1971). C1-C410 – C1-C411.
- [54] M.E. Lines, Magnetic properties of  $\text{CoF}_2$ , *Phys. Rev.* 137 (Number 3A) (1965) A982–A993.
- [55] W. Jauch, A. Palmer, A.J. Schultz, Magnetostriction in  $\text{NiF}_2$ : Combined  $\gamma$ -ray and Neutron diffraction Book – "The Application of Charge Density Research to Chemistry and Drug Design", vol. 250, Springer, 1991.
- [56] P.J. Brown, J.B. Forsyth, A neutron diffraction study of weak ferromagnetism in nickel fluoride, *J. Phys. C Solid State Phys.* 14 (Number 33) (1981) 5171–5184.
- [57] V.M. Loktev, V.S. Ostrovskii, On the theory of noncollinear magnetic structures of  $\text{CoF}_2$  in an external field, *Phys. Lett.* 99A (Number 1) (1983) 58–61.
- [58] R.I. Thomson, T. Chatterji, M.A. Carpenter,  $\text{CoF}_2$ : a model system for magnetoelastic coupling and elastic softening mechanisms associated with paramagnetic  $\leftrightarrow$  antiferromagnetic phase transitions, *J. Phys. Condens. Matter* 26 (2014) 1–13.
- [59] A.I. Belyaeva, V.V. Eremenko, N.N. Mikhailov, V.N. Pavlov, S.V. Petrov, Excitation of magnons and phonons on absorption of light in antiferromagnetic  $\text{NiF}_2$ , *Sov. Phys. - JETP* 23 (Number 6) (1966) 979–983.
- [60] K. Sujatha, S. Israel, C. Anzline, K.S. Syed Ali, R.A.J.R. Sheeba, P. Richard Rajkumar, Analysis of Oxygen bonding with metals of different oxidation states from experimental charge density distribution, *Physica B* 555 (2019) 21–31.
- [61] H. Guggenheim, The preparation of single crystals of certain transition metal fluorides, *J. Phys. Chem.* 64 (7) (1960) 938–939.
- [62] M. Barbara, Wanklyn, "The flux growth of crystals of some fluorides ( $\text{AlF}_3$ ,  $\text{CrF}_3$ ,  $\text{NiF}_2$ ,  $\text{KNiF}_3$ ,  $\text{CoF}_2$  and  $\text{KCoF}_3$ )", *J. Cryst. Growth* 5 (1969) 279–283.
- [63] International Tables for X-Ray Crystallography, vol. IV, The Kynoch Press, England, 1974.
- [64] W.H. Zachariasen, *Acta Crystallogr.* 23 (1967) 558.
- [65] S. Israel, R. Saravanan, R.K. Rajaram, Electronic structure of  $\text{InP}$  at RT, 200 and 100 K, *Physica B* 349 (2004) 390–400.
- [66] R. Saravanan, M. Prema Rani, Bonding in  $\text{CoAl}$  and  $\text{NiAl}$  metal alloys using multipole and MEM techniques, *J. Alloys Compd.* 431 (2007) 121–129.
- [67] S. Israel, K.S. Syed Ali, R.A.J.R. Sheeba, R. Saravanan, X-ray analysis of the charge density distribution in  $\text{GaP}$  at 296 and 200 K using a multipole model and the maximum entropy method, *Chin. J. Phys.* 47 (No. 3) (2009) 378–400.
- [68] M. Collins, *Nature* 298 (1982) 49.
- [69] M. Sakata, M. Sato, *Acta Crystallogr.* A46 (1990) 263.
- [70] R.A. Dilanian, F. Izumi, Super-fast Program, PRIMA, for the Maximum Entropy Method, 2005.
- [71] F. Izumi, R.A. Dilanian, Recent Research Developments in Physics, vol. 3, Transworld Research Network, Trivandrum, 2002, p. 699. Part II.
- [72] N.K. Hansen, P. Coppens, *Acta Crystallogr.* A34 (1978) 909–921.
- [73] V. Petricek, M. Dusek, L. Palatinus, The Crystallographic Computing System, Institute of Physics, Academy of sciences of the Czech republic Praha, JANA 2006, 2000.
- [74] E. Clementi, C. Roetti, Roothaan-Hartree-Fock atomic wave functions, *At. Data Nucl. Tables* 14 (1974) 177–478.
- [75] K. Momma, F. Izumi, VESTA, "visualisation for electronic and structural analysis", Commission on Crystallogr. Comput., IUCr Newsl. 7 (2006) 106.
- [76] R.F.W. Bader, *Atoms in Molecules—A Quantum Theory*, Oxford Univ. Press, Oxford, 1990.
- [77] V.G. Tsierelson, *Acta Crystallogr.* A55 (1999) Supplement, Abstract M 13-OF-003, 1999.
- [78] Adam I. Stash, Kiyooki Tanaka, Kazunari Shiozawa, Hitoshi Makino, Vladimir G. Tsirelson, "Atomic interactions in ethylenebis (1-indenyl) zirconium dichloride as derived by experimental electron density analysis", *Acta Crystallogr.* B61 (2005) 418–428.
- [79] S. Israel, K.S. Syed Ali, R.A.J.R. Sheeba, R. Saravanan, Analysis on experimental valence charge density in germanium at RT and 200K, *J. Phys. Chem. Solid.* 70 (2009) 1185–1194.
- [80] Ian Bytheway, Ronald J. Gillespie, Structures of some transition metal fluorides and oxofluorides and the VSEPR model, *J. Fluor. Chem.* 71 (1995) 189.